

Coronae & Outflows from Helical Dynamos, Compatibility with the MRI, and Application to Protostellar Disks

Eric G. Blackman

Dept. of Physics & Astronomy, Univ. of Rochester, Rochester NY, 14627, USA

Jonathan C. Tan

Princeton Univ. Observatory, Peyton Hall, Princeton, NJ 08544, USA

Abstract. Magnetically mediated disk outflows are a leading paradigm to explain winds and jets in a variety of astrophysical sources, but where do the fields come from? Since accretion of mean magnetic flux may be disfavored in a thin turbulent disk, and only fields generated with sufficiently large scale can escape before being shredded by turbulence, in situ field production is desirable. Nonlinear helical inverse dynamo theory can provide the desired fields for coronae and outflows. We discuss the implications for contemporary protostellar disks, where the MRI (magneto-rotational instability) can drive turbulence in the inner regions, and primordial protostellar disks, where gravitational instability drives the turbulence. We emphasize that helical dynamos are compatible with the magneto-rotational instability, and clarify the relationship between the two.

Keywords: outflows, dynamos, accretion disk, magnetic fields, primordial protostars

1. Introduction: the dynamo-corona-outflow paradigm

Bipolar jet-like outflows are commonly observed in protostellar systems (Richer et al. 2000), as is enhanced X-ray activity (Feigelson & Montmerle 1999). Though the correlation between outflows and X-ray activity is not entirely systematic, magnetic fields probably play an important role for both phenomena. Large scale outflows are likely magneto-centrifugally “fling” driven (Blandford & Payne 1982) or magnetically “spring” driven (e.g. Lynden-Bell 1996) from large scale open field lines, while coronal dissipation is likely the result of reconnection from closed loops, perhaps as they open (relax) to form larger scale structures. Both jet and coronal fields are plausibly the result of large scale fields produced inside protostellar disks because (1) magnetic flux is difficult to accrete in a thin turbulent disk (2) only large scale fields are able to escape from the disk before being shredded by turbulence therein. A working paradigm is this: helical dynamo \rightarrow large scale fields \rightarrow coronal fields \rightarrow field lines that relax and open up \rightarrow magnetocentrifugally launched outflow with a significant supersonic vertical velocity component \rightarrow asymptotic outflow opening angle whose tangent



© 2018 Kluwer Academic Publishers. Printed in the Netherlands.

is the ratio of the expansion speed to the vertical wind speed. The angle may be further reduced by magnetic collimation.

We focus here on understanding the principles that govern the strength of large scale disk fields produced by dynamos, and on the mechanical luminosities of the resulting winds. We do not focus on the possible role of stellar dynamos or the accretion ejection instability (Tagger & Pellat 1999; Varnière & Tagger 2002).

2. Need for in situ generation of large scale fields

2.1. SMALL SCALE FIELDS SHRED BEFORE THEY ESCAPE

For magnetic fields to launch jets or power coronae, the field buoyancy time t_b , must be $<$ its diffusion time in the disk. Since $t_b \gtrsim h/\bar{U}_b$, where h is the disk 1/2 thickness and \bar{U}_b is the buoyancy speed (\leq Alfvén speed \bar{U}_A) associated with a structure whose smallest gradient scale is L , we require $h/\bar{U}_b < L^2/\beta$ for escape, where $\beta \sim u_2 l$ is the turbulent diffusion coefficient for the magnetic field, and u_2 and l are a measure of the dominant turbulent speed and scale, where (e.g. $l \sim$ cube root of the turbulent cell volume $(l_x l_y l_z)^{1/3}$). The escape condition can be rewritten $L^2 > lh(u_2/\bar{U}_b)$ and since the ratio on the right (more on this later) is $\gtrsim u_2/\bar{U}_A \sim 1$, the condition $L^2 > lh$ is required for escape.

Now consider a Shakura-Sunyaev (Shakura & Sunyaev 1973) disk viscosity $\nu_{ss} \sim \beta = u_2 l \sim \alpha_{ss} c_s h \sim u_2^2/\Omega \sim u_{A,2}^2/\Omega$, where $u_{A,2}$ is the Alfvén speed associated with the turbulent B -field and $u_2 \sim u_{A,2}$ follows from simulations (Hawley et al. 1995; Brandenburg et al. 1995). Then $\alpha_{ss} \sim u_{A,2}^2/c_s^2$ or $u_{A,2} \sim \alpha_{ss}^{1/2} c_s$, so that $l = \alpha_{ss}^{1/2} h$. The escape condition $L^2 > lh$ then gives $L > \alpha_{ss}^{1/4} h$. Note that the minimum L applies to the *smallest* dimension of a given structure since this determines the diffusion time. This escape condition is not easily satisfied in the nonhelical MRI dynamo (see minimum k_y, k_z in fig. 3a (from Hawley et al. 1995)). More on this point later.

2.2. MEAN FLUX IS NOT FROZEN: DIFFUSION MAY BEAT ACCRETION

Can the large scale fields required by jets simply be accreted? Though 3-D MHD simulations are needed, it may be difficult for thin disks. The reason is that turbulent magnetic diffusivity $\beta \sim \nu_{ss}$ may keep the large scale field from being frozen on an advection time scale. (In general, the extent of flux freezing even for the total field depends on the turbulent spectrum. Turbulence produces many small scale structures which thus enhances the importance of the diffusion term in

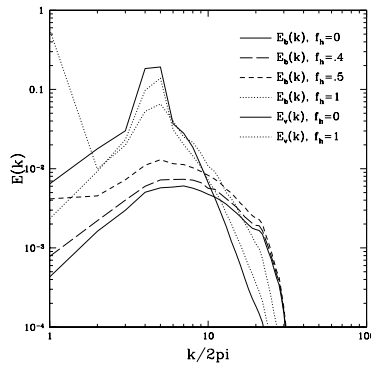


Figure 1. Saturated dynamo energy spectra (Maron & Blackman 2002).

the induction equation.) To see the potential problem, we compare the ratio of the rate of flux advection to that of diffusion. Call d the dominant vertical variation scale of the field strength. The dominant variation scale of the radial velocity is r . The above mentioned ratio is then $\nabla \times (\mathbf{v} \times \mathbf{B}) / (\beta \nabla^2 \mathbf{B}) \sim (d^2/r^2)(\alpha_{ss}hc_s/\beta)$. The diffusion term thus dominates when the plausible (though not proven) relations $d < r$ and $\alpha_{ss}hc_s \sim \beta$ apply. That diffusion can be faster than advection is supported by numerical 2-D calculation in (Lubow et al. 1994), but future 3-D numerical testing is required. This motivates an in situ helical dynamo, whose growth rate can exceed the diffusion rate.

3. MHD In Situ Amplification: Direct vs. Inverse Dynamos

We classify dynamos into two types: **direct** and **inverse**. Direct dynamo action sustains magnetic fields on scales at or below the dominant turbulent scale. This does not require helical turbulence although helicity does influence the magnetic spectrum. In contrast, inverse dynamo action describes amplification on scales larger than that of the dominant scale of the turbulence. The label “inverse” is used to suggest an inverse cascade. The turbulence must be helical to generate and sustain large scale flux over times longer than an eddy turnover time which can in turn escape to coronae and drive outflows. The distinction is illustrated in Fig 1. (Maron & Blackman 2002) for forced turbulence. The magnetic and kinetic energy spectra are plotted for different values of the fractional helicity $f_h \equiv |\mathbf{u}_2 \cdot \nabla \times \mathbf{u}_2| / |u_2^2 k_2|$. The nonhelical forcing at $k_2 = 4.5$ produces no magnetic energy at wavenumbers $k < k_2$, whereas the $f_h = 1$ case produces a large peak at $k = 1$.

3.1. DIRECT DYNAMO

For nonhelical direct dynamo action, the field grows by random walk, field line stretching (Kazantsev 1968; Parker 1979). The turbulence can be externally driven by isotropic forcing (e.g. Maron & Cowley 2002; Haugen et al. 2003), or self-generated by an angular velocity gradient (e.g. Balbus & Hawley 1998). In either case, turbulent stretching compensates for exponential decay from turbulent diffusion. The latter operates because the random motions of the gas also mix the field lines, inducing a cascade to small scales where dissipation occurs. In 3-D, a steady state balance can be achieved. In the saturated state, the magnetic energy \sim turbulent kinetic energy integrated below the dominant turbulent scale. How far the magnetic energy peak is from the forcing scale and the overall nonhelical dynamo spectrum is an active area of research (e.g. Maron & Cowley 2002; Schekochihin et al. 2002; Haugen et al. 2003), which we do not discuss further here.

3.2. HELICAL INVERSE DYNAMO

The helical inverse dynamo amplifies field on scales larger than that of the turbulence. This is most desirable for coronae and outflows. Fig 2a. shows a traditional $\alpha\Omega$ kinematic dynamo diagram (Parker 1979). Consider an initially weak toroidal (=encircling the rotation axis) loop of the magnetic field embedded in the rotator. With a vertically decreasing density gradient, a rising turbulent eddy threaded by a magnetic field will twist oppositely to the underlying global rotation to conserve angular momentum. Statistically, northern (southern) eddies twist field clockwise (counterclockwise). This is the “ α_d ” effect and the result is a large scale poloidal field loop. Differential rotation shears this loop (the “ Ω ”-effect). The bottom part reinforces the initial toroidal field and the top part diffuses away. The result is exponential growth. The α_d effect can be supplied by any source of 3-D turbulence in a stratified rotator, including gravitational instability or the MRI.

This dynamo is revealed by averaging the magnetic induction equation over a local volume and breaking all quantities (velocity \mathbf{U} , magnetic field \mathbf{B} in Alfvén velocity units, and normalized current density $\mathbf{J} \equiv \nabla \times \mathbf{B}$) into their mean (indicated by an overbar) and fluctuating (lower case) components. The result is

$$\partial_t \bar{\mathbf{B}} = \nabla \times (\alpha_d \bar{\mathbf{B}} + \bar{\mathbf{U}} \times \bar{\mathbf{B}}) + (\beta + \lambda) \nabla^2 \bar{\mathbf{B}}, \quad (1)$$

where λ is the magnetic diffusivity. The $\bar{\mathbf{U}}$ term incorporates the Ω -effect, the β term incorporates the turbulent diffusion (we assume

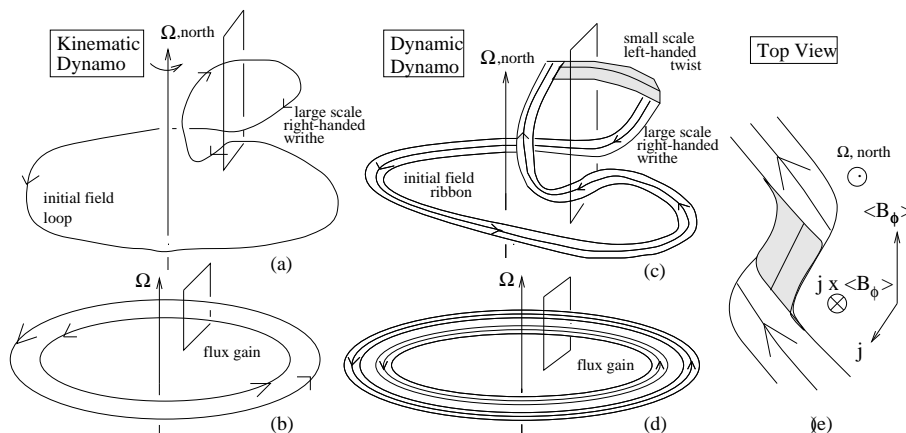


Figure 2. Kinematic helical dynamo diagram (left) ignores magnetic helicity conservation. In dynamic theory field should be replaced by ribbon, showing the conservation (Blackman & Brandenburg 2003).

constant β) and the first term on the right incorporates the α_d -effect. Accretion disk $\alpha - \Omega$ dynamo models have been proposed (Pudritz 1981; Reyes-Ruiz & Stepinski 1997;1999; Rüdiger et al. 1995; Brandenburg & Donner 1997; Campbell 1999; Rüdiger & Pipin 2000) but without a fully dynamic theory of the field saturation value. We now discuss this for forced turbulence, and expand further for disks in section 4.2.

For forced helical turbulence, α_d is (Blackman & Field 2002) $\alpha_d = \alpha_{d0} + \alpha_m$ where $\alpha_{d0} = -(\tau/3)\overline{\mathbf{u} \cdot \nabla \times \mathbf{u}}$, and $\alpha_m = (\tau/3)\overline{\mathbf{b} \cdot \nabla \times \mathbf{b}}$, where τ is a turbulent damping time. The α_m correction term arises from including the magnetic forces that backreact on the velocity (Pouquet et al. 1976; Blackman & Field 2002). From the form of α_d , it is evident that growth of α_m can offset α_{d0} and quench the dynamo (Field & Blackman 2002; Blackman & Brandenburg 2002; Blackman & Field 2002). Magnetic helicity conservation determines the dynamical suppression. The magnetic helicity, a volume integral $H \equiv \int \mathbf{A} \cdot \mathbf{B} dV \equiv \langle \mathbf{A} \cdot \mathbf{B} \rangle V$ satisfies (Woltjer 1958; Berger & Field 1984)

$$\partial_t H = -2\lambda C - \text{surface terms}, \quad (2)$$

where $\nabla \times \mathbf{A} \equiv \mathbf{B}$, and $C \equiv \langle \mathbf{J} \cdot \mathbf{B} \rangle V$. Without non-diffusive surface terms H is typically well conserved in astrophysics. Since H is a measure of field line “linkage” and “twist,” its conservation implies that the α_d -effect cannot produce a net magnetic twist, just positive and

negative magnetic twists on different scales. The conservation equations like (2) for H_1 and H_2 (where 1(2) indicates large (small) scales) are

$$\partial_t H_1 = 2S - 2\lambda k_1^2 H_1 - \text{surface terms} \quad (3)$$

$$\partial_t H_2 = -2S - 2\lambda k_2^2 H_2 - \text{surface terms}, \quad (4)$$

where $S = (\alpha_d k_1 / \epsilon - \beta k_1^2) H_1$ and $\alpha_d = \alpha_0 + \alpha_m$, where $\epsilon \leq 1$ is the fraction of the large scale field energy which is force-free. The solution without surface terms and with $\epsilon = 1$ provides an estimate for the fully helical field large scale field component, which can be further augmented by differential rotation. Because $\alpha_m \propto k_2^2 H_2$, the solution (Field & Blackman 2002; Blackman & Brandenburg 2002; Blackman & Field 2002) shows that for initially small H_2 but large α_0 , H_1 grows. Growth of H_1 implies the oppositely signed growth of H_2 . This H_2 backreacts on α_0 , ultimately quenching α_d and the dynamo.

Fig. 2a does not capture magnetic helicity conservation because a net helicity is generated. The resolution of this problem is fig. 2b (Blackman & Brandenburg 2003), where the field is treated as a ribbon. The large scale writhe corresponds to the large scale magnetic helicity and to mean field dynamo action, while the small scale twist of opposite sense along the ribbon is the result of magnetic helicity conservation. The latter twist produces a force which resists the bending of the field, and thus encapsulates the backreaction and growth of α_m . Before discussing the saturation, more on the relation between the MRI and the direct vs. inverse helical dynamos is addressed.

4. MRI is compatible with Direct and Inverse Dynamos

4.1. MRI IN NONSTRATIFIED DISK: DIRECT DYNAMO ONLY

In a sufficiently ionized disk with a weak magnetic field (note: field must be strong enough for growth to beat diffusion at critical wavenumber (Balbus & Papaloizou 1999)) the MRI results from an outward decreasing angular velocity gradient. Without vertical stratification, and thus without any pseudoscalar helicity, the MRI does not produce magnetic fields on scales larger than that of the developed turbulence. The marginally unstable (and dominant) growth mode of the MRI satisfies $ku_A \sim \Omega$ (Balbus & Hawley 1998) so that as the magnetic field is amplified from the instability, larger and larger scales become unstable to growth. The largest scale that can grow is that associated with the scale height h . Without stratification or helicity, the largest scale of the turbulent magnetic field matches the largest turbulent velocity scale (Fig. 3a (Hawley et al. 1995); k_y is the toroidal wavenumber.)

The flux associated with the field on the largest scale in the nonstratified MRI would change every turnover time as the field is shredded. The field is large scale only in the sense that the box height limits the scale of the turbulence NOT because there is any sustained ordered flux on scales larger than the turbulence. Furthermore, for a periodic box, the net flux cannot grow, as it is conserved. Note also from Fig. 3a, that the largest field structure in the vertical (k_z) and radial (k_x) directions are smaller than in the toroidal direction (k_y). This is important because the constraints of section 2.1 apply to the smallest dimension of the largest scale structures. In sum, a nonstratified nonhelical MRI does *not* produce the fields required by jets/coronae.

Nonstratified, nonhelical MRI driven turbulence and nonhelically forced turbulence behave qualitatively similarly with respect to the absence of fields on scales larger than the dominant scale of the turbulent motions. Note however, that the nonhelical MRI, *unlike* the nonhelical forced case, more nearly matches the turbulent kinetic energy spectrum on larger scales (compare the first two panels in fig. 3 to the curves in fig. 1 with $f_h = 0$). This is likely due to the fact that the global shear growth time is the same on all scales in a shearing box, and thus more able to beat diffusion on the larger scales where it can provide additional magnetic energy compared to the case without global shear.

4.2. MRI IN STRATIFIED DISK: BOTH DIRECT & INVERSE DYNAMOS

Unlike the nonstratified case, when the MRI operates in a vertically stratified medium it can have a built in inverse helical dynamo: the stratification means that turbulence produced by the MRI can be helical, in the manner discussed in section 3.2 and also from magnetic buoyancy (Brandenburg 1998; Rüdiger & Pipin 2000). One can then use a nonlinear mean field theory to model the growth and saturation of the sustained large scale flux. This is independent of the fact that the MRI will always also produce direct dynamo action that amplifies fields as described. That is, when the MRI operates in a stratified medium, one gets BOTH direct and inverse helical dynamo action.

Mean field dynamo growth is seen in magnetorotational instability simulations (Brandenburg et al. 1995, Brandenburg & Donner 1997). Fig. 3b shows a dynamo cycle in which mean flux is maintained over 30 orbits. In that simulation, large and small scale magnetic helicities are seen to have opposite sign (as expected from discussion of section 3) but $\langle \mathbf{u} \cdot \nabla \times \mathbf{u} \rangle$ has the opposite sign to $\langle \mathbf{j} \cdot \mathbf{b} \rangle$ which is not expected if $\alpha_d = \alpha_{d0} + \alpha_m$. There is an additional buoyancy term $\alpha_b \sim -\frac{\tau}{3} |g_z \langle \frac{\delta \rho}{\rho} b_x \rangle|$ (g_z is vertical gravity constant) which can exceed α_{d0} and carry the opposite sign (Brandenburg 1998; Rüdiger & Pipin 2000). Then, for

example, in the northern hemisphere $\alpha_d \sim -\tau|g_z\langle(\delta\rho/\rho)b_x\rangle| + |\tau\langle\mathbf{v} \cdot \nabla \times \mathbf{v}\rangle|/3 + \tau\langle\mathbf{j} \cdot \mathbf{b}\rangle/3$. The 1st and 2nd terms on the right have opposite signs and the sign of the large scale magnetic helicity is determined by whichever of those two initially dominates (since α_d is the growth coefficient). This then predicts the sign of the last term on the right, which grows with opposite sign to the large scale magnetic helicity, eventually quenching the larger of the 1st two terms on the right.

The fact that the stratified MRI leads to both helical dynamo action and direct dynamo action, whereas the nonstratified MRI leads only to direct dynamo action is the key to clarifying previous discussions of the MRI and the traditional mean field dynamo: It is sometimes stated that even a nonstratified MRI generates “large scale” fields without the need for helical turbulence. But this statement relates directly to section 4.1. The fields referred to as “large scale” in this nonhelical context are just the result of direct (not helical) dynamo action: 1) they only reach the maximum scale of the turbulence, not larger, and 2) they change the sign of their flux every eddy turnover time (every rotation period). That such fields are generated without helicity, does not make the MRI inconsistent with helical dynamos: as discussed above, when stratified turbulence is present both direct dynamo and inverse helical dynamos operate together and large scale fields on scales larger than that of the dominant turbulence arise.

Like Brandenburg et al. (1995), Stone et al. (1996), studied the stratified MRI. But the latter used vertically periodic boxes so no net flux could grow. Flux could have appeared in each $\frac{1}{2}$ of the Stone et al. (1996) box with opposite sign, but this was not a large region, given the resolution: Measuring finite pseudoscalars in a periodic stratified box requires averaging only over $\frac{1}{2}$ of the vertical thickness, since the sign changes across the midplane. For a periodic stratified box, the pseudoscalars must vanish at the midplane and at the top and bottom.

5. Helical Dynamo Saturation in Disks & Outflow Power

The helical dynamo grows helical large scale field first “kinematically” (independent of dissipation and with growth rate not too different from α_{d0}) until $|\alpha_m| \sim |\alpha_b - \alpha_{d0}|$, after which the field growth is resistively limited. Setting $|\alpha_m| \sim |\alpha_b - \alpha_{d0}|$, and using magnetic helicity conservation, then provides a reasonable estimate of the helical field by the end of the kinematic phase. Growth beyond that value is often too slow to be of interest. The large scale helical field at the end of the kinematic phase is (Blackman & Field 2002; Tan & Blackman 2003)

$$\overline{B}_H \sim (4\pi\rho f_h)^{1/2} u_2 (l/h)^{1/2} \simeq (4\pi\rho)^{1/2} \alpha_{ss} c_s, \quad (5)$$

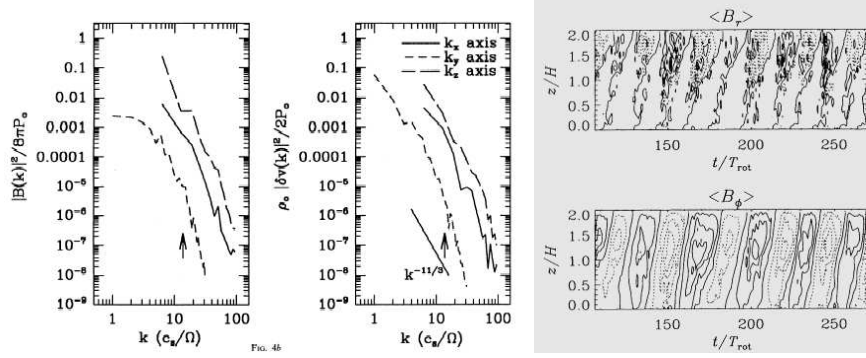


Figure 3. (a) Nonhelical MRI spectra from Hawley et al. (1995) and (b) MRI driven helical dynamo cycle in stratified non-periodic box (Brandenburg & Donner 1997).

where f_h is the fractional kinetic helicity, l is the dominant turbulent scale, h is the disk height (=the vertical scale of the growing mean field), and the latter similarity follows for disks since $l/h \sim \alpha_{ss}^{1/2}$ and $u_2 \sim \alpha_{ss}^{1/2} c_s$, which in turn follow from the scalings of section 2.1.

Eqn. (5) is an estimate of the helical field but the nonhelical toroidal field is further amplified by shear. The toroidal field is linearly stretched above \overline{B}_r during a buoyancy time scale. The buoyancy loss time is $\tau_b \sim h(4\pi\rho)^{1/2}/\overline{B}_\phi$, so linear growth of \overline{B}_ϕ above (5) in a time τ_b gives $\overline{B}_\phi = \overline{B}_r \Omega \tau_b = \alpha_{ss}^{1/2} c_s (4\pi\rho)^{1/2}$ so $\overline{B}_r/\overline{B}_\phi = \alpha_{ss}^{1/2}$.

The above mean fields have their smallest variation scale $\sim h$ and thus satisfy the conditions of section 2.1 and can rise to the corona, open up, and launch outflows. By using $\nabla \cdot \overline{\mathbf{B}}$ one can use the disk field to estimate the field at the surface and the Poynting flux there (Tan & Blackman 2003). This provides an estimate for the magnetic luminosity available for magneto-centrifugal (Blandford & Payne 1982) or magnetic “spring” (Lynden-Bell 1996) driven outflows

$$L_{mag} \sim \frac{c}{4\pi} \int (\overline{\mathbf{E}} \times \overline{\mathbf{B}}) \cdot d\mathbf{S} \sim \frac{\alpha_{ss}^{1/2} G m_* \dot{m}_*}{r} \quad (6)$$

$$\simeq 220 L_\odot \left(\frac{\alpha_{ss}}{10^{-2}} \right)^{1/2} \frac{m_*}{M_\odot} \frac{\dot{m}_*}{10^{-2} M_\odot / \text{yr}} \left(\frac{10^{13} \text{cm}}{r} \right),$$

using normalizations for primordial protostars (Tan & McKee 2003).

6. Outflows in Contemporary & Primordial Protostars

The time scale for which the helical dynamo operates at a given radius is not the viscous time, but the accretion disk’s lifetime (\sim star formation time). This is because the mean field is NOT frozen into the flow. The

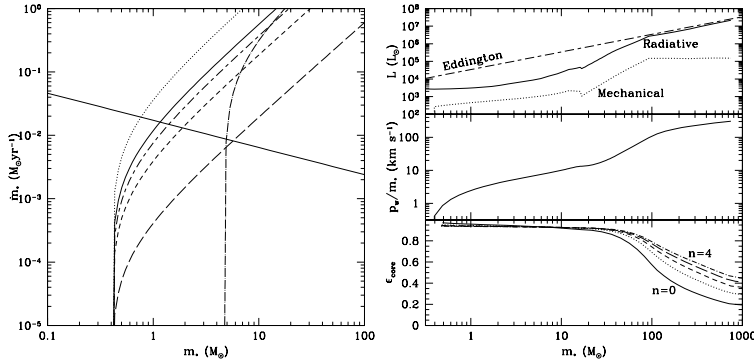


Figure 4. (a) Dynamo saturation regime for primordial protostellar disks (b) Evolution of radiative and wind mechanical luminosities from protostar and disk; outflow momentum; effect of wind on star formation efficiency (Tan & Blackman 2003).

amplification is statistical, lasting as long as turbulence is supplied. For contemporary star formation, we expect that growth to the kinematic saturation value occurs in a small fraction of the star formation time, since the initial fields after collapse from molecular clouds are already quite strong and the star formation time scales are relatively long. Contemporary protostellar disks should be able to easily sustain outflows powered by fields from a helical dynamo, with the helical turbulence in the inner regions of the disk supplied by the MRI.

For primordial protostellar disks, although magnetic Reynolds numbers are high, the seed fields are weaker and the MRI may be unfavorable for the maximally unstable mode. Instead, gravitational instability (Gammie 2001, Wada et al. 2002; though these are 2-D simulations) may supply the 3-D helical turbulence for much of the dynamo evolution. In addition, we expect the star formation time scales to be relatively short since the accretion rates are $\sim 10^{-2} M_\odot/\text{yr}$ (Tan & McKee 2003). Gravitational instability in the disk may maintain the Toomre parameter $Q \lesssim 1$ (Gammie 2001; Tan & Blackman 2003): Where the disk is initially stable (such that viscosity is small), mass accumulates, triggering the instability. This can induce turbulent accretion rather than global angular momentum transport (e.g. Gammie 2001). Typical accretion rates, while large by contemporary standards, are small enough that fragmentation is not expected (Tan & Blackman 2003).

Tan & Blackman (2003) used a primordial protostellar model (Tan & McKee 2003) to determine the m_* vs. \dot{m}_* regime for which a helical dynamo reaches the end of the kinematic regime (discussed above). In Fig. 4a., the rising curves mark the condition where the helical field has been able to saturate, as the disk is old enough to have allowed

sufficient dynamo amplification. The disk dynamo is assumed to start operating once the centrifugal radius of the accretion flow is \sim twice the stellar radius, which happens when $m_{*,\text{init}} = 0.4M_{\odot}$ in the fiducial case. The dashed, solid, and dotted lines show the saturation condition for $\alpha_{\text{ss}} = 10^{-3}, 10^{-2}, 0.1$, all with radius $r = 10^{13}$ cm and seed field of 10^{-16} G. With $\alpha_{\text{ss}} = 0.01$, the long-dashed line shows the condition at $r = 10^{14}$ cm, the dashed-long-dashed line shows it for a seed field of 10^{-26} G, and the dot-long-dashed line shows it evaluated with $m_{*,\text{init}} = 4.7M_{\odot}$, corresponding to a more slowly rotating initial gas core.

Protostellar growth starts from low masses with accretion rates that decline with time (and so also with protostellar mass), as shown by the straight thick solid line. In the fiducial case the field in the inner disk saturates when $m_* \sim 1M_{\odot}$. This does not depend sensitively on α_{ss} . In lower angular momentum cores the disk emerges later and the dynamo then rapidly saturates. The main message of Fig 4a is that dynamo saturation and thus dynamo-driven winds may occur at relatively low protostellar masses, even in the primordial case.

Fig. 4b (Tan & Blackman 2003) shows the evolution of protostellar luminosities (radiative and mechanical), the cumulative specific outflow momentum relative to stellar mass (assuming that the wind speed is the escape speed from the protostellar surface and that the flow kinetic energy dominates far from the star), and the resulting star formation efficiency due to erosion of the core by the outflow for the fiducial case of Fig 4a, with $\alpha_{\text{ss}} = 0.01$. The efficiency calculation is based on Matzner & McKee (1999,2000). The initial core's axisymmetric angular density profile is specified by $dM/d\Omega = (1/4\pi)Q(\mu)M$, with $\mu = \cos\theta$ and $Q(\mu) = (1 - \mu^2)^n / \int_0^1 (1 - \mu^2)^n d\mu$. The solid line is $n = 0$ (isotropic core), dotted is $n = 1$, dashed is $n = 2$, long-dashed is $n = 3$, dot-dashed is $n = 4$. The message from fig. 4b is that dynamo driven winds can strongly affect the star formation efficiency for masses $m_* \gtrsim 100M_{\odot}$, at which the protostar has contracted to the main sequence radius, and the contraction has enhanced the accretion and wind luminosities.

References

- Balbus, S. A., & Hawley, J. F. 1998, *Rev. Mod. Phys.*, 70, 1
 Balbus, S. A. & Papaloizou, J. C. B. 1999, *ApJ*, 521, 650
 Berger, M., & Field, G. B. 1984, *J. Fluid Mech.*, 147, 133
 Blackman, E.G., 2003, in proceedings of the 1st Niels Bohr Summer Institute: "Beaming and Jets in Gamma-Ray Bursts", Copenhagen, Aug 2002, edited by R. Ouyed, J. Hjorth & A. Nordlund, astro-ph/0211187
 Blackman, E. G. & Brandenburg, A. 2002, *ApJ*, 579, 359
 Blackman, E. G. & Brandenburg, A. 2003, *ApJL*, 584, L99

- Blackman, E. G., & Field, G. B. 2002, Phys. Rev. Lett., 89, 265007
- Blandford, R. D. & Payne, D. G. 1982, MNRAS, 199, 883.
- Brandenburg, A, 1998, in *Theory of Black Hole Accretion Disks* M. A. Abramowicz, G. Bjornsson, and J. E. Pringle eds. (Cambridge University Press) p.61
- Brandenburg, A. 2001, ApJ, 550, 824
- Brandenburg, A., Nordlund, A., Stein, R. F., & Torkelsson, U. 1995, ApJ, 446, 741
- Brandenburg, A. & Donner, K. 1997, MNRAS, 288, L29
- Campbell, C. G. 1999, MNRAS, 310, 1175
- Feigelson, E. D., & Montmerle, T. 1999, Ann. Rev. A. & A., 37, 363
- Field, G.B., & Blackman, E.G. 2002, ApJ, 572, 685
- Gammie, C. F. 2001, ApJ, 553, 174
- Haugen, N.E.L, Branendburg A., Dobler W., 2003, sub. to PRL, astro-ph/0303372.
- Hawley, J.F., Gammie C.F. & Balbus, S.A., 1995, ApJ 440, 742
- Kazantsev, A.P., 1968, Sov. Phys., JETP, 26 1031
- Konigl, A. & Pudritz, R. E. 2000, Protostars and Planets IV, 759
- Lubow, S. H., Papaloizou, J. C. B., & Pringle, J. E. 1994, MNRAS, 267, 235
- Lynden-Bell D., 1996, MNRAS, 279, 389
- Maron J. & Cowley S., 2002, sub. to ApJ, astro-ph/0111008.
- Maron J. & Blackman E.G., 2002, ApJL 556, L41.
- Matzner, C. D., & McKee, C. F. 1999, ApJ, 526, 109
- Matzner, C. D., & McKee, C. F. 2000, ApJ, 545, 364
- Moffatt, H. K. 1978, *Magnetic Field Generation in Electronically Conducting Fluids* (Cambridge, UK: Cambridge University Press)
- Ouyed, R., Clarke, D. A., & Pudritz, R. E. 2003, ApJ, 582, 292
- Parker, E. N., 1979, *Cosmical Magnetic Fields* (Oxford: Clarendon Press).
- Pouquet, A., Frisch, U., & Léorat, J. 1976, J. Fl. Mech., 77, pt. 2, 321 (PFL)
- Pudritz, R. E. 1981, MNRAS, 195, 897
- Reyes-Ruiz, M. & Stepinski, T. F. 1997, MNRAS, 285, 501
- Reyes-Ruiz, M. & Stepinski, T. F. 1999, A. & Ap., 342, 892
- Richer, J., Shepherd, D., Cabrit, S., Bachiller, R., & Churchwell, E. 2000, in *Protostars & Planets IV*, eds. V. Mannings, A. P. Boss, & S. S. Russell (Tucson: The University of Arizona Press), 867
- Rüdiger, G., Elstner, D., & Stepinski, T. F. 1995, A. & Ap., 298, 934
- Rüdiger, G. & Pipin, V. V. 2000, A. & Ap., 362, 756
- Schekochihin, A. A., Cowley, S. C., Hammett, G. W., Maron, J. L., & McWilliams, J. C. 2002, New Journal of Physics, 4, 84
- Shakura N.I. & Sunyaev R.A., 1973, A& A., 24, 337
- Stone, J. M., Hawley, J. F., Gammie, C. F., & Balbus, S. A. 1996, ApJ, 463, 656
- Tagger, M. & Pellat, R. 1999, A. & Ap, 349, 1003
- Tan, J.C. & Blackman E.G., 2003, in prep.
- Tan, J.C. & McKee C.F., 2003, in prep.
- Tout C.A. & Pringle J.E., MNRAS, 281, 219
- Varnière, P. & Tagger, M. 2002, A. & Ap., 394, 329
- Wada, K., Meurer, G., & Norman, C. A. 2002, ApJ, 577, 197
- von Rekowski, B., Brandenburg, A., Dobler, W., & Shukurov, A. 2003, A. & Ap., 398, 825
- Woltjer, L., 1958, Proc. Nat. Acad. Sci., 44 489.